Journal of King Saud University - Science 35 (2023) 102986

HOSTED BY

Contents lists available at ScienceDirect

Journal of King Saud University - Science

journal homepage: www.sciencedirect.com

Aloe vera mucilage as an eco-friendly corrosion inhibitor for bronze in chloride media: Combining experimental and theoretical researches

Bouchra Benzidia [a,*], Mohammed Barbouchi [b], Malak Rehioui [a], Hind Hammouch [a], Hamid Erramli [a], Najat Hajjaji [a]

[a] Laboratory of Organic Chemistry, Catalysis and Environment, Department of Chemistry, Faculty of Sciences, Ibn Tofail University, BP 133, 14000 Kenitra, Morocco
[b] Laboratory of Molecular Chemistry and Natural Substances, Department of Chemistry, Faculty of Sciences, Moulay Ismail University, B.P 11201 Zitoune, Meknes, Morocco

ARTICLE INFO

Keywords:
Aloe vera (L.) Burm. F.
Mucilage
Bronze B66
Corrosion inhibitor
3% NaCl

ABSTRACT

Aloe vera (*L.*) *Burm.F.* (=*Aloe barbadensis Mill.*), a widely recognized medicinal plant, holds a prominent position due to its potent cosmetic and medicinal attributes. The objective of this work is to develop a new eco-friendly corrosion inhibitor for bronze B66 that is non-toxic, simple to apply, cost-effective, stable, and reversible. To achieve this goal, we initially devised an improved and cost-efficient method for extracting *Aloe vera* mucilage (AVM). Then we tested as corrosion inhibitor for bronze B66 in 3 % NaCl using gravimetric measurements, electrochemical methods and Scanning Electron Microscopy (SEM) coupled with Energy Dispersive X-Ray analysis (EDX). The electrochemical assessments validated the findings from the gravimetric analysis and demonstrated that our inhibitor significantly modifies the electrochemical process mechanism at the B66/3% NaCl interface. The corrosion rate of bronze decreases with the inhibitor's presence, and its inhibitory effectiveness amplifies with higher concentrations, reaching an efficiency of 86 % at 750 ppm. The mechanism of metallic copper and corrosion Acemannan inhibitor was explored through DFT studies and molecular dynamics simulation.

1. Introduction

Corrosion, a gradual phenomenon, poses a threat to the structural stability of diverse sectors like transportation, chemical, petrochemical, and construction. The speed of corrosion hinges on environmental factors, the metal's composition, and its inherent properties. Regrettably, it is frequently overlooked during the design phase, resulting in direct expenses for replacements and labor, alongside indirect expenses such as decreased production and efficiency. Additionally, in heritage preservation, corrosion contributes to the vanishing of historical artifacts and distortion of archaeological records (Liu and Chen, 2023; Qu et al., 2022).

Metallic materials, especially copper and its alloys, for example bronze, are highly exposed to corrosion, whether they come into contact with humid atmospheres, immersed in fresh or saline water. The marine environment (solution 3 % NaCl) is particularly aggressive towards these materials (Alcántara et al., 2017).

The use of corrosion inhibitors to prevent the process of metal dissolution remains an inevitable and widespread application (Al-Amiery and Al-Azzawi, 2023). Many inorganic inhibitors (those containing phosphate, chromate, and other heavy metals), or synthetic organic inhibitors (extensively applied) proved an excellent corrosion inhibiting potential in the corrosive environments. A large part of them are now being gradually restricted or prohibited by various environmental regulations, because of their toxicity, which pose serious problems for human health and raise major ecological problems (Chigondo and Chigondo, 2016).

Recently, research studies in the different fields (science and engineering) are directed towards for research and development of environmental friendliness chemical species to replace traditional toxic corrosion inhibitors (Verma et al., 2021a). Therefore, due to environmental concerns, medicinal and aromatic plants are increasingly established as one of the most effective and profitable source of green corrosion inhibitors (Alrefaee et al., 2021; Barbouchi et al., 2020b, 2019; Boussalem et al., 2023; Chaubey et al., 2021; Popoola et al., 2023; Salleh et al., 2021), because of their efficiency, economy, ecology and

* Corresponding author.
E-mail address: benzidia1511@gmail.com (B. Benzidia).

https://doi.org/10.1016/j.jksus.2023.102986
Received 25 November 2021; Received in revised form 16 October 2023; Accepted 31 October 2023
Available online 1 November 2023

environment-friendly.

Aloe vera (L.) Burm.F. (=*Aloe barbadensis Mill.*) is a widely known as a medicinal plant, belong to Xanthorrhoeaceae family or also to the subfamily of Asphodelaceae, according to the classification APGIII phylogenetics (Kumar et al., 2017), it is one of the most powerful and best known for its cosmetic and medicinal properties plants (Liu et al., 2019).

The majority of current research on the significant inhibition of plant extract as a corrosion inhibitor derive from *Aloe vera*, was focused on corrosion control of metals or their alloys in acidic (HCl or H_2SO_4) medium (Abiola and James, 2010; Ayoola et al., 2020; Dahiya et al., 2016; Eddy and Odoemelam, 2009; Kumar and Yadav, 2018; Mehdipour et al., 2015; Singh et al., 2016; Sribharathy et al., 2013).

With the exception of our previous study (Benzidia et al., 2019); on the use of tannins extract obtained from the green rind of *Aloe vera* as a green inhibitor, for the corrosion inhibition of bronze B66 in 3 % NaCl. In the literature, we can not find any solid information about possible applications of the *Aloe vera* extract on the corrosion of the metals or their alloys corrosion in neutral media (3 % NaCl).

The above-mentioned points, inspired our team to examine the use of *Aloe vera* mucilage (AVM) as a corrosion inhibitor in a 3 % NaCl against bronze B66. *Aloe vera* mucilage present in the succulent leaves of *Aloe vera* plant consists of about 98.5–99.5 % water, the remaining solids being composed mainly of polysaccharides (~60 % w/w), in particular the bioactive polymer Acemannan. This polysaccharide (Acemannan) is mainly composed of partially acetylated mannose units linked by β-(1 → 4) glycosidic bonds (Minjares-Fuentes et al., 2017).

The novelty of our research lies in the utilization of a biomaterial as an environmentally friendly corrosion inhibitor. Specifically, we employ *Aloe vera* mucilage in a powdered form, which is obtained through a recently patented process (Benzidia et al., 2018).

In order to do this, an experimental and theoretical investigation has been performed to evaluate corrosion inhibition property of AVM in powder form on bronze B66 corrosion in 3 % NaCl. The inhibition performance was provided via electrochemical measurements (stationary and transient). Surface characterizations, including SEM and EDX were conducted. Furthermore, the theoretical modeling was carried out using MD and DFT techniques to explore the adsorption of the Acemannan inhibitor over the metal surface.

2. Material and methods

2.1. Materials and sample preparation

The working electrode we used is a synthetic bronze B66 of similar composition in archaeological bronze; a copper alloy with 4.87 % tin, see Table S1.

The corrosive solution consists of an aerated solution of sodium chloride (30 g/L) prepared by dissolving NaCl Merck in distilled water.

The biomaterial, *Aloe vera* mucilage in powder form obtained by a new-patented process (Benzidia et al., 2018).

2.2. Gravimetric study

Gravimetric study is widely used because it has the advantage of being simple and does not require a large apparatus. In this study, we performed the gravimetric test by measuring mass loss after 24 h of immersion. In order to get corrosion rate W ($g.cm^{-2}.h^{-1}$) the formula (1) is used:

$$w = \left[\frac{m_i - m_f}{S.t}\right] \quad (1)$$

The inhibition efficiency (η_{WL} (%)) was calculated by Eq. (2):

$$\eta_{WL}(\%) = \left[\frac{W^{\circ} - W}{W^{\circ}}\right] \times 100 \quad (2)$$

S: surface of the part (cm^2); t: time (hour); m_i: weighing of the initial weight; m_f: mass after test; W° and W are the corrosion rates of the sample after immersion in the solution without and with inhibitor, respectively.

2.3. Electrochemical experiments

2.3.1. Stationary techniques

The potentiodynamic polarization (PDP) curves were obtained using a three-electrode assembly; a platinum electrode used as a counter-electrode, an XR300/XR310 reference electrode Ag/AgCl, and the working electrode which is made of cylindrical bronze B66 (1 cm^2 of surface area). The stationary measurements were made in potentiodynamic mode using a Bio-logic Science instruments potentiostat/galvanostat SP-200. The work electrode is kept previously immersed in the corrosion-free potential for one hour. The chosen sweep speed is 1 mV/s.

The determination of the electrochemical parameters (i_{corr}, E_{corr}, β_a and β_c) was established from the polarization curves, using the EC-Lab software. Thus, the inhibition efficiency (η_{PDP} (%)) was computed by using the following Eq. (3):

$$\eta_{PDP}(\%) = \left[1 - \frac{i_{corr}}{i^{\circ}_{corr}}\right] \times 100 \quad (3)$$

where i°_{corr} and i_{corr} are corrosion current densities values without and with inhibitor, respectively.

2.3.2. Transient techniques

The electrochemical impedance spectroscopy (EIS) diagrams were plotted using the same SP-200 stationary measurement device, with a signal amplitude of 10 mV. The range of frequencies explored varies from 100 KHz to 10 mHz. As regards the inhibition efficiency (η_{EIS} (%)) was computed by the Eq. (4):

$$\eta_{EIS}(\%) = \left[1 - \frac{R_P}{R_{P(inh)}}\right] \times 100 \quad (4)$$

where the $R_{p(inh)}$ and R_p represent the transfer resistance with and without the addition of inhibitor, respectively.

2.4. Surface analysis techniques by SEM/EDX

The morphological characterization of the surface of the bronze coupons was carried out at the Moroccan Foundation for Advanced Science, Innovation and Research (MAScIR), by a field emission scanning electron microscope (SEM) and by energy dispersion. The X-ray spectroscopy, EDX (Bruker model 6130 flash X) is performed by FEI microscopy (model quanta FEG 450).

2.5. Quantum chemical calculations

Density Functional Theory (DFT) based quantum chemical calculations were performed on the Acemannan using using the DMol3 module embedded in the Material Studio (MS, version 7.0) program of Accelrys Inc. They were calculated based on generalized gradient approximation (GGA) of Perdew–Burke Ernzerhof (PBE) and "double numeric plus polarization" (DNP, setting to 4.4) (Chugh et al., 2020). All DFT calculations have been done in aqueous phase (water) using COSMO controls. Indeed, the electronic inhibitors properties analysed here include several theoretical indices: the values of frontier molecular orbitals (E_{LUMO} and E_{HOMO}), energy band gap (ΔE_{gap}), electron affinity (E_A), ionization potential (I_P), electronegativity (χ), chemical potential (μ), hardness (η), electrophilicity index (ω), and softness (σ). The computational parameters can be calculated from the values of E_{HOMO} and E_{LUMO} using following relations given below (Barbouchi et al., 2020a; Domingo et al., 2016; Tan et al., 2020).

$$\Delta E_{gap} = E_{LUMO} - E_{HOMO} \quad (5)$$

$$\chi = \frac{I_P + E_A}{2} \quad (6)$$

$$\eta = \frac{I_p - E_A}{2} \quad (7)$$

where the $I_p = -E_{HOMO}$ and $E_A = -E_{LUMO}$.

$$\omega = \frac{\mu^2}{2\eta} \quad (8)$$

where the electronic chemical potential $\mu = ((E_{LUMO} + E_{HOMO})/2)$.

$$\sigma = \frac{1}{\eta} \quad (9)$$

The Fukui functions (FIs) are obtained through the finite difference approximation using Hirschfeld Population Analysis (HPA). The FIs or nucleophilic and electrophilic attacks are obtained from the following approximations (Geerlings et al., 2003):

$$f_K^+(r) = \rho_k(N+1) - \rho_k(N) \quad \text{Nucleophilic attack} \quad (10)$$

$$f_K^-(r) = \rho_k(N) - \rho_k(N-1) \quad \text{Electrophilic attack} \quad (11)$$

In the above equations, $\rho_k(N)$, $\rho_k(N-1)$ and $\rho_k(N+1)$ are the atomic charges of the systems with N, $N+1$, and $N-1$ electrons, respectively.

2.6. Molecular dynamics simulations

The Forcite module performed in Materials Studio software was employed to estimate the nature of the interaction between the Acemannan inhibitor (Table 5) and the copper sorbent. For this purpose, the Cu crystal was imported, then cleaved alongside (1 1 1) plane and a slab of 8 Å was utilized. The surface of Cu (1 1 1) was relaxed by minimizing its energy employing the smart minimizer method. As well as the surface of Cu (1 1 1) was enlarged to a (22 × 22) supercell in order to envisage a wide surface for the interaction of studied inhibitors. Then, a vacuum slab of 20 Å thickness was constructed above the Cu (1 1 1) plane. A supercell composing of 2000 H_2O, 20 NaCl molecules was added and finally we create the molecules of the tested Acemannan. As regards to simulation was achieved via a simulation box in the NVT canonical ensemble at 298 K with a time step of 0.1 fs and simulation time of 300 ps carried out at 298 K, NVT ensemble, as well as COMPASS force field. In simulation system, the interactions and binding energies of the Acemannan inhibitor with the Cu (1 1 1) surface were estimated by using the following equations (Li et al., 2021):

$$E_{interaction} = E_{total} - (E_{surface+solution} + E_{inhibitor}) \quad (12)$$

$$E_{bindinig} = -E_{interaction} \quad (13)$$

where E_{total} represents the total energy of the system, $E_{surface+solution}$ counted as a measure of the total energy of Cu (1 1 1) surface and solution devoid of Acemannan inhibitor and $E_{inhibitor}$ the total energy of Acemannan inhibitor.

3. Results and discussion

3.1. Gravimetric study

Measurements of weight loss are a first approach to studying the corrosion inhibition of a metal in an electrolytic solution. This method has the advantage of simple implementation and the unnecessary need for extensive equipment.

Table 1 gives the values of the corrosion rate and the percentage of the η_{WL} calculated by gravimetry, without and with different concentrations of AVM, and this after 24 h of immersion in 3 % NaCl against bronze B66 specimens.

Table 1
Corrosion rate and inhibition efficiency as a function of inhibitor concentrations.

	W (g/h.cm^2)	η_{wt} (%)
NaCl 3 %	3.70×10^{-5}	–
250 ppm	1.47×10^{-5}	60.27
500 ppm	1.30×10^{-5}	64.86
750 ppm	7.04×10^{-6}	80.97

Analysis of the results obtained (Table 1), clearly shows that the AVM have properties that inhibit the corrosion of bronze B66 in a 3 % NaCl medium.

It can be observed that when adding these mucilage to the corrosive medium, the corrosion rate decreases significantly, while η_{WL} increases (reaches a value of 80,97 %) with increasing AVM concentration, which is due to the increase in the surface area covered by the inhibitor molecules of the adsorbed AVM relative to the active sites of the bronze B66 surface.

3.2. Electrochemical study

3.2.1. Open circuit potential

Fig. S2 represents the change in bronze B66 time-related potential in 3 % NaCl, in absence and presence of AVM at different concentrations.

In the absence of the AVM inhibitor, the corrosion potential of bronze B66 in 3 % NaCl undergoes a variation in the first minutes, and after 2500 s it stabilizes towards − 0.165 V. This can be attributed to the formation of a layer of corrosion products on the metal surface.

In the presence of 250 ppm and 500 ppm AVM, we observed a decrease in the corrosion potential towards negative values at immersion for both concentrations. This displacement would be the consequence of the delay of the cathodic reaction of dissolution of bronze B66 due to the action of *Aloe vera* mucilage. Although the presence of 750 ppm in AVM, the corrosion potential moves on the contrary, towards a positive value with a well marked stability from 3000 s. This evolution of the potential indicates that the inhibition effect at 750 ppm acts preferentially on the anodic process.

3.2.2. Polarization curves

The polarization curves are obtained in potentiodynamic mode, and this after one hour of immersion of the bronze B66 electrode in NaCl 3 %, in absence and presence of AVM at different concentrations. The results achieved are represented in Fig. 1a (cathodic domain) and Fig. 1b (anodic domain).

Cathode curves (Fig. 1a); in the absence of AVM inhibitor, a rapid increase in the current density in the vicinity of corrosion potential then tends to stabilize to a value of the order of 0.1 mA/cm^2, corresponding to the oxygen diffusion limit current.

The addition of AVM at different concentrations causes a significant decrease in current density in the vicinity of E_{corr}. This decrease is more pronounced when the concentration of AVM inhibitor increases. It is accompanied by a shift of the corrosion potential towards more negative values. For potentials greater than −0.45 V, we notice the appearance of a linear part reflecting an exponential variation of the current. This area becomes wider when the inhibitor concentration increases. There is also an observed limit current that corresponds to the oxygen reduction for all concentrations.

Anode curves (Fig. 1b); the addition of the inhibitor in the aggressive solution leads to a significant decrease in the value of the corrosion current density for the concentration 750 ppm of AVM. Thus, the corrosion current density increases from 9.48 μA.cm^{-2} in the case of the control to 0.59 μA.cm^{-2} at a concentration of 750 ppm of AVM. Therefore, in this concentration, we note the appearance of a passivation step in a broad field of potential, the extent of the passive zone reaches a minimum current density. This indicates that the protective film formed

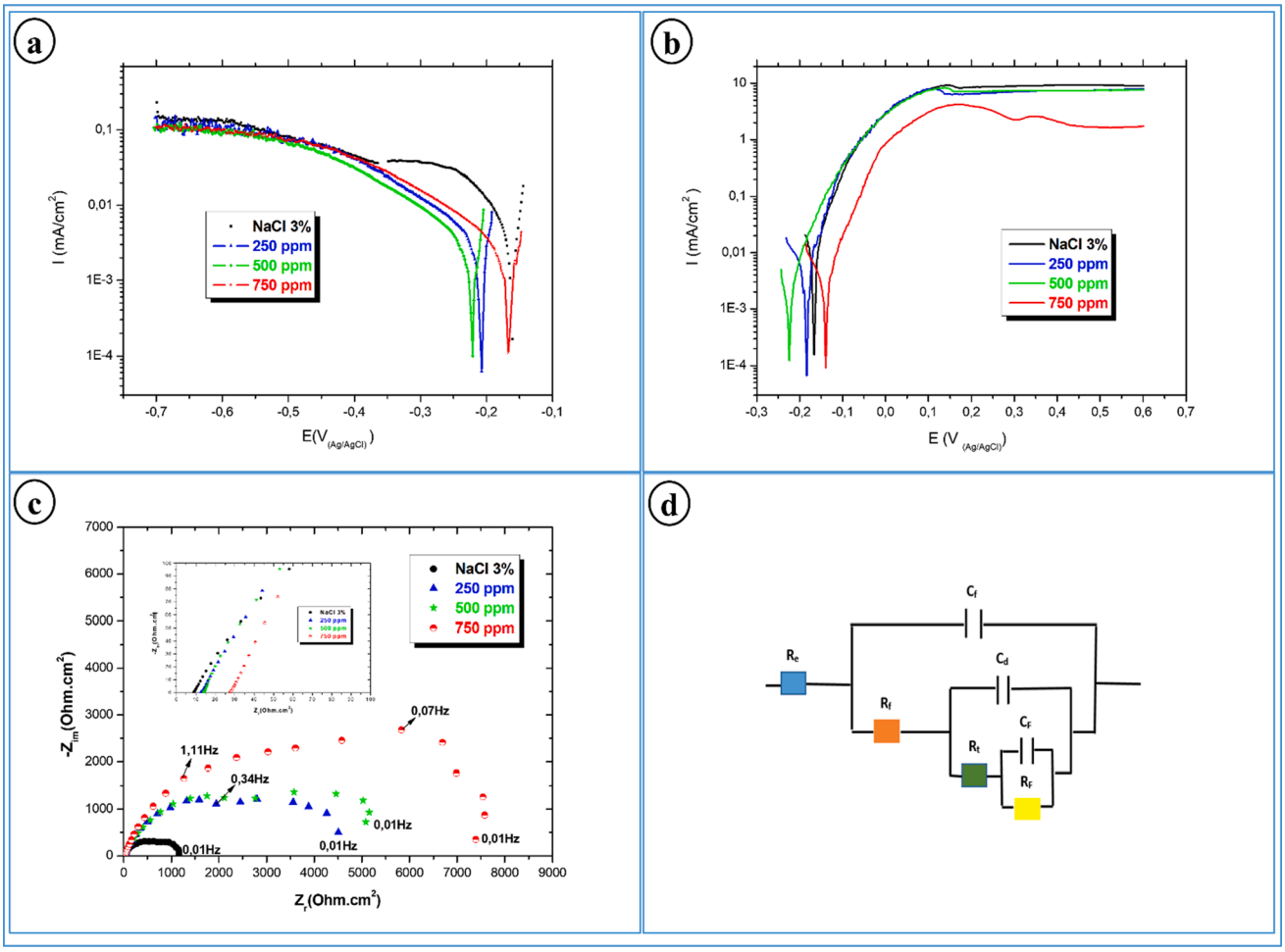

Fig. 1. Cathodic polarization curves (a), anodic polarization curves (b), electrochemical impedance diagrams (c), and electrical circuit used to fit the electrochemical impedance diagrams (d), of bronze in 3% NaCl solution without and with different concentration of AVM.

on the electrode surface adheres and acts as a barrier against the surface's accessibility to chloride ions (Chauhan et al., 2019).

From the electrochemical parameters collected in Table 2, it is found that the increase in concentration leads to a decrease in the value of the current density. Inhibition efficacy reaches a value of around 94 % at a concentration of 750 ppm AVM. In addition, the anodic and cathodic slopes of Tafel were modified by adding the AVM, demonstrating that the molecules of this mucilage affect both the anodic and cathodic reactions. Then, the difference in E_{corr} value is very less than 85 mV, which indicates that the inhibitor molecules of the AVM are mixed type inhibitors (Aouniti et al., 2018; Li et al., 2021).

3.2.3. *Electrochemical impedance measurements*

In order to explore the surface characters of bronze B66, EIS measurements for bronze in 3 % NaCl solution without and with different concentrations of AVM inhibitor, after one hour of immersion, were conducted. Likewise, in order to extract qualitative information, fit the impedance data using *EC-Lab* software. It is performed to model the EIS spectra and electrical equivalent circuit (EEC) is composed of 3RC in parallel (presented in Fig. 1d). In this mode of EEC, R_e represent the electrolyte resistance R_f stands for inhibitors film resistance C_f is the capacity representing the dielectric property of the film, R_t is the charge transfer resistance, C_d represents the double-layer capacity, R_F is the faradic resistance of corrosion products accumulated on metal surface, and the C_F stands for faradic capacity of the oxidation process of corrosion products. The Nyquist plots and their electrochemical parameter of bronze B66 immersed in the inhibited and uninhibited corrosive solution are given in Fig. 1c and Table 3, respectively.

For blank, the impedance spectra (Fig. 1c) displayed the appearance of two capacitive loops. A weakly flattened capacitive loop at high frequencies, attributed to the transfer of charge which controls the interfacial process and whose polarization resistance is of the order of 1143 Ωcm^2. A dispersion at low frequencies linked to the transport of matter.

The addition of the AVM inhibitor at different concentrations shows

Table 2
Electrochemical parameters drawn from bronze B66 polarization curves in NaCl 3% in absence and presence of AVM.

		Cathodic domain			Anodic domain			η_{PDP} (%)
		$-E_{corr}$ (mV)	I_{corr} (μA.cm^{-2})	β_c (mV)	$-E_{corr}$ (mV)	I_{corr} (μA.cm^{-2})	β_a (mV)	
NaCl 3 %		165.8 ± 3.3	9.5 ± 0.1	63.4	152.5 ± 3.1	9.48 ± 0.1	41.6	–
MUCAV(ppm)	250	207.1 ± 1.0	1.35 ± 0.01	49.6	182.4 ± 0.9	4.19 ± 0.02	39.7	85.75
	500	220.1 ± 1.1	0.74 ± 0.01	32.0	224.4 ± 1.1	0.81 ± 0.01	20.7	92.08
	750	165.7 ± 0.8	0.65 ± 0.01	34.8	138.0 ± 0.6	0.59 ± 0.01	10.7	94.09

Table 3
Electrochemical parameters derived from electrochemical impedance diagrams.

	R_e ($\Omega.cm^2$)	R_f ($\Omega.cm^2$)	C_f ($\mu F/cm^2$)	R_t ($\Omega.cm^2$)	C_d ($\mu F/cm^2$)	R_F ($\Omega.cm^2$)	C_F ($\mu F/cm^2$)	R_P ($\Omega.cm^2$)	η_{EIS} %
NaCl 3 %	8.91	–	–	703	147.9	440	860	1143 ± 22	–
250 ppm	12.83	9.28	115	3412	4.78	1273	227	4694 ± 23	75.64
500 ppm	13.53	51.75	109	3523	0.87	1975	143	5550 ± 27	79.40
750 ppm	25.75	54.51	82.77	5683	0.74	2392	141	8130 ± 40	85.94

the appearance of three capacitive loops with a significant increase in polarization resistance.

At high frequencies, the size of the capacitive loop increases with concentration. This change in the pitch of the impedance diagrams can be attributed to a change in the interfacial process as the concentration increases (Rahmouni et al., 2007).

At medium frequencies, the inhibitory effect results in an increase in the value of the load transfer resistance R_t, which shows a significant variation depending on the inhibitor concentration. It reaches a maximum of 5683 $\Omega.cm^2$ at a concentration of 750 ppm.

At low frequencies, the R_F value increases and C_F decreases with the concentration of AVM, and this will make the surface film thicker which shows well the protective effect of our inhibitor on the interface bronze B66/3%NaCl.

From Table 3, it can be noted that the R_F resistance increases with the inhibitor concentration, it goes from 440 $\Omega.cm^2$ in the absence of an inhibitor to 2392 $\Omega.cm^2$ with 750 ppm of AVM. This can only be explained by the formation of a film on the surface of the electrode. The inhibitory efficiency increases with the inhibitor concentration and reaches 85.94 % for a concentration of 750 ppm AVM. These results are in good agreement with those from stationary polarization curves and weight-loss measurements.

3.3. SEM/EDX analysis

Fig. 2 shows the surface morphology map of the bronze B66 sample after soak in 3 % NaCl solution for 24 h at 298 K: (a) the surface morphology in 3 % NaCl solution, (b) the surface morphology with 750 ppm of AVM. This SEM micrograph plan view is coupled with EDX analysis to determine the elements present on the bronze B66 surface without and with the addition of AVM inhibitor.

As shown in Fig. 2a, the appearance of a clear attack at the surface of the bronze due to chloride ions, which causes pitting corrosion. The elemental EDX analysis of this sample shows the presence of oxygen and chlorine in addition to the major elements (Cu, Sn and Pb). This favors the formation of corrosion products, which would be mainly in the form of copper oxide and chlorides. In contrast, the bronze surface containing 750 ppm of AVM in Fig. 2b, the attack is much less marked, confirming the inhibition effect of the latter by the presence of an inhibitory film on the bronze surface, the EDX analysis reveals the presence of carbon, and a remarkable reduction of oxygen. The important carbon signal certainly corresponds to the carbon chains of AVM.

3.4. Quantum chemistry study

The Quantum chemical calculations is one of the most useful methods to analyze the inhibitor/surface interactions, which can efficaciously predict whether inhibitor compounds can exhibit potential corrosion inhibition performance.

In order to correlate the inhibition efficacy found experimentally with the electronic properties of the major compound Acemannan ($C_{66}H_{100}NO_{49}$) from AVM. We evaluated the reactivity of Acemannan in

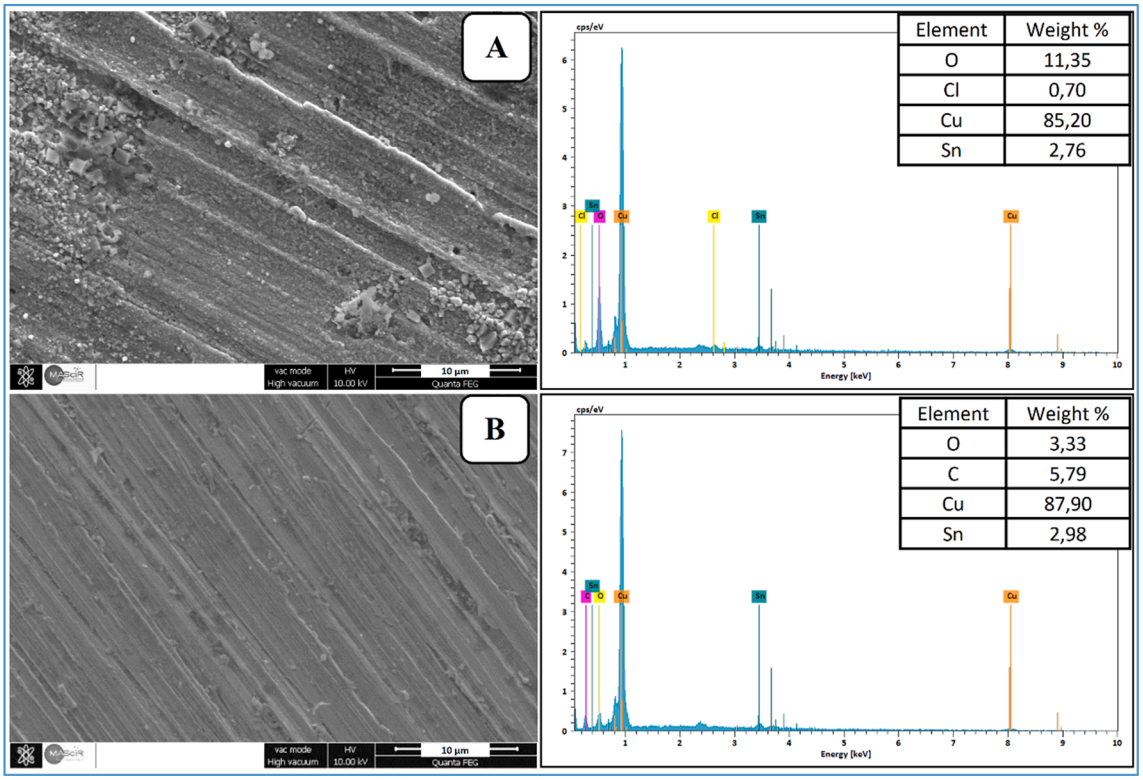

Fig. 2. SEM/EDX of bronze B66 samples after immersing in 3 % NaCl environment for 24 h: (a) SEM/EDX in blank solution, (b) SEM/EDX with 750 ppm of AVM.

its neutral and protonated forms. This biopolymer has several oxygen atoms (49 atoms) and a single nitrogen atom capable of protonation. Therefore, it is evident that the most favorable site for protonation is the nitrogen atom of Acemmanan.

Optimization of the structure of neutral and protonated forms of Acemmanan, their electron density distributions of frontier molecular orbitals (HOMO and LUMO), and distributions of nucleophilic attacks, while electrophilic attacks are illustrated in Fig. 3. The electronic indices (E_{LUMO}, E_{HOMO}, ΔE_{gap}, E_A, I_P, χ, μ, η, ω, σ), and the Fukui indices (f^- and f^+) are shown in Tables 4 and S3, respectively.

From Fig. 3, it can be found that the HOMO electron cloud in neutral forms of Acemmanan is distributed on the nitrogen atom and the oxygen atoms (O1, O11, and O39) around it. While the electron cloud of LUMO is distributed on the oxygen (O9)-containing six-membered ring and the carboxylic acid group attached to the adjacent carbon atom of that oxygen atom. As regards the protonated form of Acemmanan, the electron cloud of HOMO is distributed on the six-membered ring containing oxygen (O24) and the oxygen of the hydroxy, methoxy and carbonyl groups attached to the carbon atoms of this ring, as well as the oxygen atoms O14, O18 and O37. The LUMO electron cloud is mainly distributed on the protonated nitrogen and the adjacent oxo group.

From this distribution of HOMO and LUMO orbitals, it is agreed that the reactive sites of HOMO orbitals on neutral and protonated forms of Acemmanan, can give electrons to form coordination bonds with metals. Therefore, the active sites of the LUMO orbitals can accept electrons from metals to form feedback bonds. Considering that, HOMO orbital corresponds to the electron donating capacity of as inhibitor molecule, whereas, LUMO orbital match the electron-accepting capacity of as inhibitor molecule (He et al., 2021).

The energy gap (ΔE_{grap}) value indicates the energy deficit, is another important parameter that provides conclusive information on the strength of the corrosion inhibition capacity of a corrosion inhibitor molecule. The lower the ΔE_{grap} value, the greater the interaction between the inhibitors and the metal surface, which can be explained by the fact that the adsorption action between the inhibitors and the metal surface increases as the value of ΔE_{grap} decreases (Saha et al., 2016). The ΔE_{grap} values for neutral and protonated forms of Acemmanan are 3,813 and 2,728 eV, respectively. Therefore, the protonated form of Acamannan has better corrosion inhibition performance than its neutral form.

The χ parameter is related to chemical potential, and the high value of χ indicates better inhibitory performance (Barbouchi et al., 2020a). On the other hand, electron donation starting from the inhibitors to metal, increases with the increasing the σ and decreases with increasing the η of the inhibitor, in other words, the lowest values of η mean more polarisability and inhibition efficiency (Haldhar et al., 2018). This favours the protonated form over the neutral form of Acemannan (see Table 5).

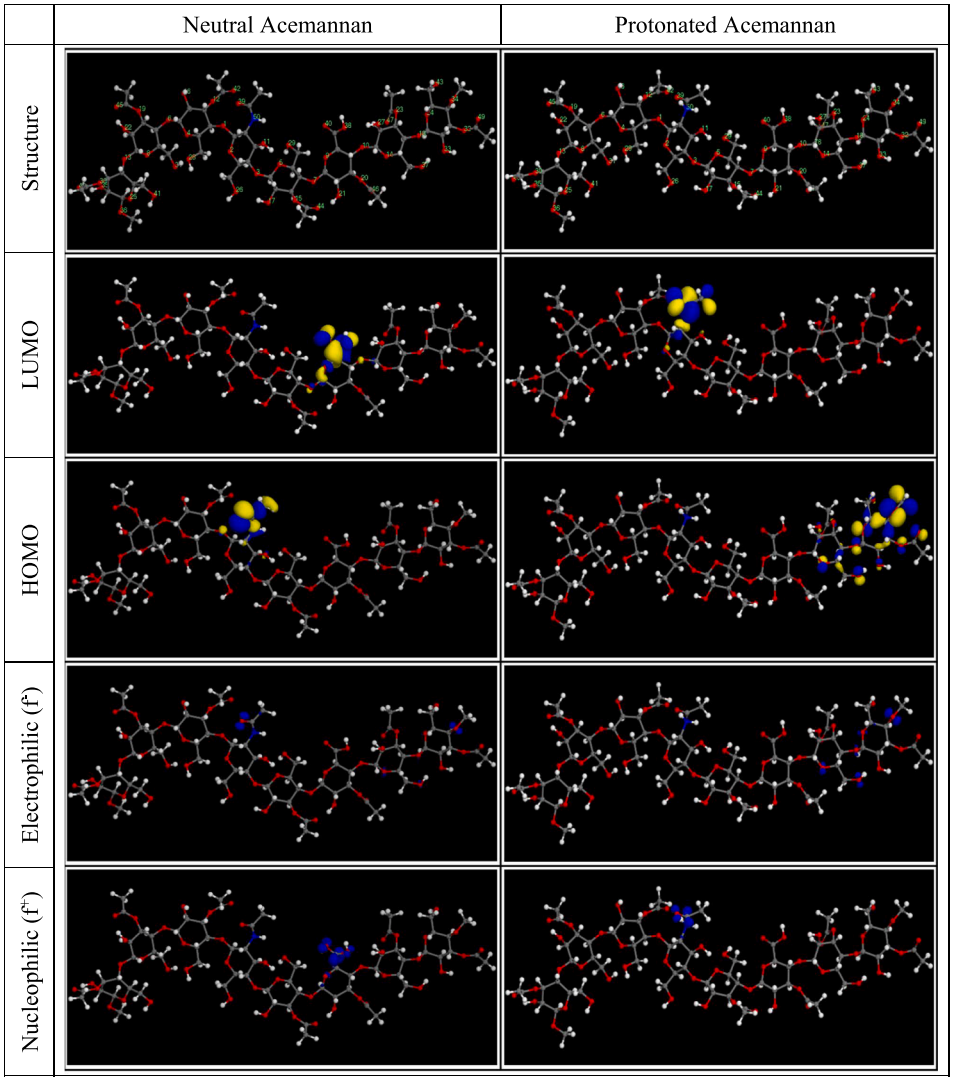

Fig. 3. Optimized molecular structure, frontiers molecular orbitals and Fukui functions distributions of neutral and protonated Acemannan.

Table 4
The HOMO and LUMO energies (eV), energy gap (ΔE_{gap}), electron affinity (E_A), ionization potential (I_P), electronegativity (χ), chemical potential (μ), hardness (η), electrophilicity (ω), and softness (σ) of neutral and protonated Acemannan compound.

Inhibitor name	E_{LUMO} (eV)	E_{HOMO} (eV)	ΔE_{gap} (eV)	E_A (eV)	I_p (eV)	χ (eV)	μ (eV)	η (eV)	ω (eV)	σ (eV)$^{-1}$
Neutral Acemannan	−1.993	−5.806	3.813	1.993	5.806	3.899	−3.899	1.906	3.987	0.525
Protonated Acemannan	−3.174	−5.942	2.768	3.174	5.942	4.558	−4.558	1.384	7.506	0.723

Table 5
Interaction and binding energies obtained from MD simulation for neutral and protonated Acemannan compound adsorbed on Cu (1 1 1) surface.

Simulations models	$E_{interaction}$ (KJ/mol)	$E_{binding}$ (KJ/mol)
Neutral Acemannan	−2981.43	2981.43
Protonated Acemannan	−3129.42	3129.42

The ω index is a measure of the stabilization of energy, after a system accepts an additional electronic charge of another species (Verma et al., 2021b). From the resulting data (see Table 4), the protonated form of Acemannan, carries the lowest value of the μ followed by the highest value of the ω index from where Acemannan in its protonated form, promotes its electrophilic behavior.

It is agreed that a molecule that has high values of the function centers of Fukui, is considered chemically more reactive (Berrissoul et al., 2020). Which means we can identify the reactive sites that are responsible for the electrophilic and nucleophilic attacks of the Acemannan in neutral and protonated forms. From the Fig. 3 and the results grouped in Table S3 it can be seen that, for the neutral Acemannan, the high values of f^- are located on the O14, O34, O37, O39 and N50 atoms which are electron-donating (responsible for the electrophilic attacks). While the high f^+ values of the O9, O38 and O40 atoms are capable of receiving electrons (nucleophilic attacks). For the protonated Acemannan, electron-donating are O14, O18, O24, O34, and O37 atoms, indicating that the protonation influences the local electron-donating selectivity. On the other hand, the electron acceptor atoms are N50 and O39 with the most intense value of f^+, which shows that the acceptor power of the protonated Acemannan is more privileged.

3.5. Molecular dynamics simulation

The most stable adsorption configurations of neutral and protonated Acemannan on Cu (1 1 1) surface in the presence of 2000 H_2O and 20 NaCl molecules was simulated using Molecular dynamics simulation and is shown in Fig. 4.

From Fig. 4, it is evident that protonated Acemannan, which exhibited the strongest interaction and by extension the highest inhibition efficiency, lies flat and completely parallel on the Cu (1 1 1) surface, which leads to a stronger interaction. Whereas the neutral Acemannan is approximately parallel with varying angles of oblique deflection when interacting with the iron surface. This leads to reduced interactions with the copper surface.

It is clear from the results obtained in Table 5 that the adsorption energies of Acemannan on the copper surface increased from the neutral form to the protonated form. The highest negative adsorption energy indicates the system with the most stable and strongest adsorption. The $E_{binding}$ values of neutral and protonated Acemannan are 2981.43 kJ/mol and 3129.42 kJ/mol, respectively. Therefore, protonated Acemannan exhibiting better corrosion inhibition performance than neutral Acemannan. The trend is in agreement with the results of inhibition efficiency obtained by the quantum chemistry calculations for both forms of

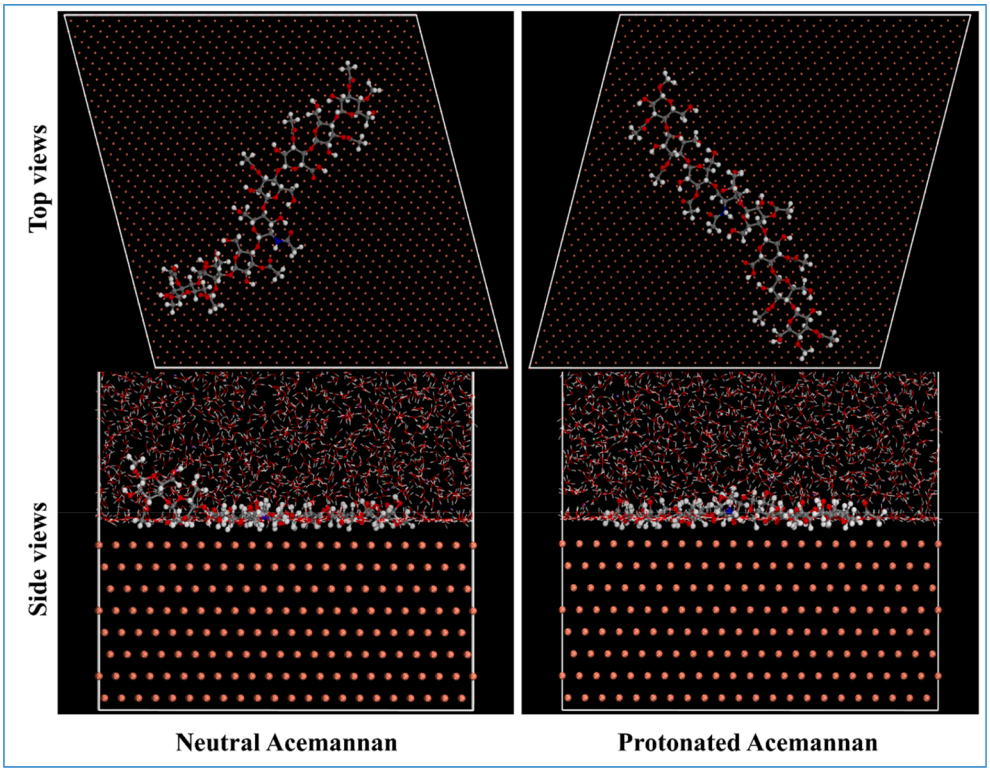

Fig. 4. Side and Top views of the most stable configurations for the adsorption of neutral and protonated Acemannan over Cu (1 1 1) surface obtained from MD simulations.

acemannan.

4. Conclusion

In this study, AVM in powder form as an eco-friendly corrosion inhibitor was successfully prepared by a new-patented process. Combined with experimental and theoretical techniques, the corrosion inhibition performance of AVM for bronze in 3 % NaCl were investigated.

The weight loss assessments indicate that the AVM efficiently hinders bronze corrosion in a 3 % NaCl environment. The inhibition efficiency rises in tandem with higher AVM concentrations. Both polarization and EIS investigations corroborate the effectiveness of AVM as a corrosion inhibitor for bronze in 3 % NaCl. The polarization study also reveals that AVM functions as a mixed-type inhibitor. SEM/EDX analysis shows that the AVM inhibitor adsorb on bronze surface and protect the bronze surface against chlorides. The theoretical study of the bioactive polymer Acemannan (major polysaccharide of AVM), under neutralization and protonation conditions show that both quantum chemistry calculations and MD simulations are in agreement. Which proved that protonated Acemannan exhibiting better corrosion inhibition performance than neutral Acemannan.

These findings support the utilization of natural products as environmentally friendly corrosion inhibitors. Furthermore, they appear promising and practical for the application of our AVM inhibitor in the preservation of bronze archaeological artifacts showcased in museums.

Declaration of competing interest

The authors declare that they have no known competing financial interests or personal relationships that could have appeared to influence the work reported in this paper.

Appendix A. Supplementary material

Supplementary material to this article can be found online at https://doi.org/10.1016/j.jksus.2023.102986.

References

Abiola, O.K., James, A.O., 2010. The effects of Aloe vera extract on corrosion and kinetics of corrosion process of zinc in HCl solution. Corros. Sci. 52, 661–664. https://doi.org/10.1016/j.corsci.2009.10.026.

Al-Amiery, A.A., Al-Azzawi, W.K., 2023. Mannich bases as corrosion inhibitors: An extensive review. J. Mol. Struct. 1294, 136421 https://doi.org/10.1016/j.molstruc.2023.136421.

Alcántara, J., Fuente, D.d.l., Chico, B., Simancas, J., Díaz, I., Morcillo, M., 2017. Marine atmospheric corrosion of carbon steel: A review. Materials (Basel) 10 (4), 406. https://doi.org/10.3390/ma10040406.

Alrefaee, S.H., Rhee, K.Y., Verma, C., Quraishi, M.A., Ebenso, E.E., 2021. Challenges and advantages of using plant extract as inhibitors in modern corrosion inhibition systems: Recent advancements. J. Mol. Liq. 321, 114666 https://doi.org/10.1016/j.molliq.2020.114666.

Aouniti, A., Azzouzi, M.E., Belfilali, I., Warad, I.K., Elmsellem, H., Hammouti, B., Jama, C., Bentiss, F., Zarrouk, A., 2018. Anticorrosion potential of new synthesized naphtamide on mild steel in hydrochloric acid solution: gravimetric, electrochemical, surface morphological, UV-visible and theoretical investigations. Anal. Bioanal. Electrochem. 10, 1193–1210.

Ayoola, A.A., Fayomi, O.S.I., Akande, I.G., Ayeni, O.A., Agboola, O., Obanla, O.R., Abatan, O.G., Chukwuka, C.J., 2020. Inhibitive corrosion performance of the eco-friendly aloe vera in acidic media of mild and stainless steels. J. Bio- Tribo-Corros. 6, 1–13. https://doi.org/10.1007/s40735-020-00361-y.

Barbouchi, M., Benzidia, B., Idrissi, M.E., Choukrad, M., 2019. *Pistacia lentiscus* L. essential oils as a green corrosion inhibitors for iron in neutral chloride media. Anal. Bioanal. Electrochem. 11, 333–348.

Barbouchi, M., Benzidia, B., Aouidate, A., Ghaleb, A., El Idrissi, M., Choukrad, M., 2020a. Theoretical modeling and experimental studies of Terebinth extracts as green corrosion inhibitor for iron in 3 % NaCl medium. J. King Saud Univ. – Sci. 32, 2995–3004. https://doi.org/10.1016/j.jksus.2020.08.004.

Barbouchi, M., Benzidia, B., El Idrissi, M., Choukrad, M., 2020b. Iron corrosion green inhibition in a 3% NaCl solution, by leaves extract from Pistacia terebinthus L. Growing wild in Morocco. Port. Electrochim. Acta 38, 175–184. https://doi.org/10.4152/pea.202003175.

Benzidia, B., Hajjaji, N., Hammouch, H., Belahbib, N., 2018. Procédé d'extraction de mucilage d'Aloe Vera. MA 39394, B1.

Benzidia, B., Hammouch, H., Dermaj, A., Benassaoui, H., Abbout, S., Hajjaji, N., 2019. Investigation of green corrosion inhibitor based on aloe vera (L.) burm. F. for the protection of bronze B66 in 3% NaCl. Anal. Bioanal. Electrochem. 11, 165–177.

Berrissoul, A., Ouarhach, A., Benhiba, F., Romane, A., Zarrouk, A., Guenbour, A., Dikici, B., Dafali, A., 2020. Evaluation of Lavandula mairei extract as green inhibitor for mild steel corrosion in 1 M HCl solution. Experimental and theoretical approach. J. Mol. Liq. 313, 113493 https://doi.org/10.1016/j.molliq.2020.113493.

Boussalem, O., El Bouazzaoui, Y., Habsaoui, A., El Amri, A., Mhanni, D., Doumane, G., Dkhireche, N., Ebn Touhami, M., 2023. The study of the methanolic extract of "Pelargonium gravelons" as a green corrosion inhibitor of mild steel in H2SO4 0.5 M. Chem. Data Collect. 48, 101084 https://doi.org/10.1016/j.cdc.2023.101084.

Chaubey, N., Savita, Qurashi, A., Chauhan, D.S., Quraishi, M.A., 2021. Frontiers and advances in green and sustainable inhibitors for corrosion applications: A critical review. J. Mol. Liq. 321, 114385.

Chauhan, D.S., Kumar, A.M., Quraishi, M.A., 2019. Chemical Engineering Research and Design Hexamethylenediamine functionalized glucose as a new and environmentally benign corrosion inhibitor for copper. Chem. Eng. Res. Des. 150, 99–115. https://doi.org/10.1016/j.cherd.2019.07.020.

Chigondo, M., Chigondo, F., 2016. Recent natural corrosion inhibitors for mild steel: An overview. J. Chem. 2016, 1–7.

Chugh, B., Singh, A.K., Chaouiki, A., Salghi, R., Thakur, S., Pani, B., 2020. A comprehensive study about anti-corrosion behaviour of pyrazine carbohydrazide: Gravimetric, electrochemical, surface and theoretical study. J. Mol. Liq. 299, 112160 https://doi.org/10.1016/j.molliq.2019.112160.

Dahiya, S., Lata, S., Kumar, P., Kumar, R., 2016. A descriptive study for corrosion control of low-alloy steel by Aloe vera extract in acidic medium. Corros. Rev. 34, 241–248. https://doi.org/10.1515/corrrev-2016-0015.

Domingo, L.R., Ríos-Gutiérrez, M., Pérez, P., 2016. Applications of the conceptual density functional theory indices to organic chemistry reactivity. Molecules 21, 1–22. https://doi.org/10.3390/molecules21060748.

Eddy, N.O., Odoemelam, S.A., 2009. Inhibition of corrosion of mild steel in acidic medium using ethanol extract of Aloe vera. Pigment Resin Technol. 38, 111–115. https://doi.org/10.1108/03699420910940617.

Geerlings, P., De Proft, F., Langenaeker, W., 2003. Conceptual density functional theory. Chem. Rev. 103, 1793–1873. https://doi.org/10.1021/cr990029p.

Haldhar, R., Prasad, D., Saxena, A., 2018. Myristica fragrans extract as an eco-friendly corrosion inhibitor for mild steel in 0.5 M H2SO4 solution. J. Environ. Chem. Eng. 6, 2290–2301. https://doi.org/10.1016/j.jece.2018.03.023.

He, J., Yu, D., Xu, Q., Li, G., Chen, G., An, J., Yang, J., Li, W., 2021. Combining experimental and theoretical researches to insight into the anti-corrosion property of Morinda citrifolia Linn leaves extracts. J. Mol. Liq. 325, 115145 https://doi.org/10.1016/j.molliq.2020.115145.

Kumar, S., Yadav, M., Yadav, A., Yadav, J.P., 2017. Impact of spatial and climatic conditions on phytochemical diversity and in vitro antioxidant activity of Indian Aloe vera (L.) Burm.f. S. Afr. J. Bot. 111, 50–59. https://doi.org/10.1016/j.sajb.2017.03.012.

Kumar, H., Yadav, V., 2018. International Journal of Innovative Research in Science, Engineering and Technology. Asian J. Chem. 26, 70–73.

Li, H., Zhang, S., Qiang, Y., 2021. Corrosion retardation effect of a green cauliflower extract on copper in H2SO4 solution: Electrochemical and theoretical explorations. J. Mol. Liq. 321, 114450 https://doi.org/10.1016/j.molliq.2020.114450.

Liu, F., Chen, L., 2023. Thiadiazoles as potent inhibitors against corrosion of metals and alloys: Challenges and future prospects. J. Mol. Liq. 390, 122904 https://doi.org/10.1016/j.molliq.2023.122904.

Liu, C., Cui, Y., Pi, F., Cheng, Y., Guo, Y., Qian, H., 2019. Extraction, purification, structural characteristics, biological activities and pharmacological applications of acemannan, a polysaccharide from aloe vera: A review. Molecules 24 (8), 1554.

Mehdipour, M., Ramezanzadeh, B., Arman, S.Y., 2015. Electrochemical noise investigation of Aloe plant extract as green inhibitor on the corrosion of stainless steel in 1M H2SO4. J. Ind. Eng. Chem. 21, 318–327. https://doi.org/10.1016/j.jiec.2014.02.041.

Minjares-Fuentes, R., Medina-Torres, L., González-Laredo, R.F., Rodríguez-González, V. M., Eim, V., Femenia, A., 2017. Influence of water deficit on the main polysaccharides and the rheological properties of Aloe vera (Aloe barbadensis Miller) mucilage. Ind. Crops Prod. 109, 644–653. https://doi.org/10.1016/j.indcrop.2017.09.016.

Popoola, L.T., Yusuff, A.S., Ikumapayi, O.M., Chima, O.M., Ogunyemi, A.T., Obende, B. A., 2023. Carbon steel behavior towards Cucumeropsis mannii shell extract as an ecofriendly green corrosion inhibitor in chloride medium. Sci. Afr. 21, e01860. https://doi.org/10.1016/j.sciaf.2023.e01860.

Qu, Z., Wang, X., Shen, X., Zhou, H., 2022. Study of the Cu(111) surface by scanning tunneling microscopy: The morphology evolution, reconstructions, superstructures and line defects. Nanomaterials 12, 4278. https://doi.org/10.3390/nano12234278.

Rahmouni, K., Hajjaji, N., Keddam, M., Srhiri, A., Takenouti, H., 2007. The inhibiting effect of 3-methyl 1,2,4-triazole 5-thione on corrosion of copper in 3% NaCl in presence of sulphide. Electrochim. Acta 52, 7519–7528. https://doi.org/10.1016/j.electacta.2006.12.079.

Saha, S.K., Dutta, A., Ghosh, P., Sukul, D., Banerjee, P., 2016. Novel Schiff-base molecules as efficient corrosion inhibitors for mild steel surface in 1 M HCl medium: Experimental and theoretical approach. Phys. Chem. Chem. Phys. 18, 17898–17911. https://doi.org/10.1039/c6cp01993e.

Salleh, S.Z., Yusoff, A.H., Zakaria, S.K., Taib, M.A.A., Abu Seman, A., Masri, M.N., Mohamad, M., Mamat, S., Ahmad Sobri, S., Ali, A., Teo, P.T., 2021. Plant extracts as green corrosion inhibitor for ferrous metal alloys: A review. J. Clean. Prod. 304, 127030 https://doi.org/10.1016/j.jclepro.2021.127030.

Singh, A.K., Mohapatra, S., Pani, B., 2016. Corrosion inhibition effect of Aloe Vera gel: Gravimetric and electrochemical study. J. Ind. Eng. Chem. 33, 288–297. https://doi.org/10.1016/j.jiec.2015.10.014.

Sribharathy, V., Rajendran, S., Rengan, P., Nagalakshmi, R., 2013. corrosion inhibition by an aqueous extract of Aloe vera (L.) Burm F. (Liliaceae). Eur. Chem. Bull. 2, 471–476.

Tan, B., Zhang, S., Qiang, Y., Li, W., Li, H., Feng, L., Guo, L., Xu, C., Chen, S., Zhang, G., 2020. Experimental and theoretical studies on the inhibition properties of three diphenyl disulfide derivatives on copper corrosion in acid medium. J. Mol. Liq. 298, 111975 https://doi.org/10.1016/j.molliq.2019.111975.

Verma, C., Ebenso, E.E., Quraishi, M.A., Hussain, C.M., 2021a. Recent developments in sustainable corrosion inhibitors: Design, performance and industrial scale applications. Mater. Adv. 2, 3806–3850. https://doi.org/10.1039/d0ma00681e.

Verma, D.K., Kaya, S., Ech-chihbi, E., El-Hajjaji, F., Phukan, M.M., Alnashiri, H.M., 2021b. Investigations on some coumarin based corrosion inhibitors for mild steel in aqueous acidic medium: Electrochemical, surface morphological, density functional theory and Monte Carlo simulation approach. J. Mol. Liq. 329, 115531 https://doi.org/10.1016/j.molliq.2021.115531.